Development of a Space-Charge Transport Model for Ion-Exchange Membranes

A two-dimensional, electrokinetic transport model that incorporates ionic hydration, orientation of solvent molecules by an applied electric field, and solvent dipole-dipole interactions is developed. The model is used to simulate equilibrium and transport experiments for perfluorosulfonic acid membranes containing aqueous alkali metal sulfate solutions. The membrane is modeled as an array of cylindrical pores. Solution of the mathematical model requires that the membrane porosity, water partition coefficient, coion partition coefficient, water diffusion coefficients, and coion and counterion diffusion coefficients be known. Membrane coion and counterion diffusion coefficients were determined from free solution equivalent conductance data. All other parameters were determined experimentally for a Nafion (of E. I. du Pont de Nemours Inc.) cation-exchange membrane and five 0.1 M alkali metal sulfate solutions. Experimental radiotracer data for coion absorption as well as for coion and water transport are compared with theoretical predictions to test the accuracy of the model.

Angel G. Guzmán-Garcia
Peter N. Pintauro
Department of Chemical Engineering
Tulane University
New Orleans, LA 70118

Mark W. Verbrugge
Physical Chemistry Department

Robert F. Hill
Analytical Chemistry Department
General Motors Research Laboratories
Warren, MI 48090

Introduction

Ion-exchange membranes are used widely in a number of electrochemical devices, including batteries, fuel cells, electrochemical sensors, and electrochemical reactors. In spite of their importance, scientists and engineers do not fully understand the behavior of mobile species within ion-exchange membranes. Three questions can be posed which illustrate the crux of our current lack of understanding:

1. When an ion-exchange membrane equilibrates with a reservoir in which it is placed, what final concentration of solvent and ionic species inhabit the membrane, and what basic principles can be postulated to describe this equilibrium state?

2. During nonequilibrium conditions in which solvent and ionic species are transported, which phenomena govern the rates of motion and why do some ions of similar charge transport at different rates?

3. How does the nonuniform, microscopic pore structure of the polymer matrix affect solvent and ion absorption in and transport through an ion-exchange membrane?

Despite considerable theoretical and experimental work performed over the past three decades attempting to answer these fundamental questions, an accurate description of these phenomena has not yet emerged. It is generally accepted that the ability of an ionic species to absorb in and transport through an ion-exchange membrane is governed by molecular level interactions among the solute, solvent, and membrane matrix. Sufficiently detailed micro-level mathematical models for solute and solvent absorption in and transport through an ion-exchange membrane would be of great value to polymer engineers and membrane researchers who are developing new membrane separation applications and formulating new membrane polymer materials. Such detailed models could be used to: 1. propose new membrane structures with specific ion and solvent transport characteristics; and 2. simulate the performance of a given membrane in a particular electrochemical device or separation process.

A variety of mathematical models have been proposed to describe transport in neutral and ion-exchange membranes. One such mathematical approach consists of using *capillary* or *electrokinetic* transport models which regard an ion-exchange membrane as an array of parallel cylindrical pores of constant radius with a uniform distribution of ion-exchange sites on the pore walls. When the pore radius is of the same order of magnitude as the Debye screening length, electroneutrality

within the pore is no longer valid. The existence of a nonzero space charge region results in coupling between electrical forces, mass transfer, and fluid flow in the pore. Such electrokinetic phenomena have been incorporated mathematically into numerous analyses of membrane transport; a comprehensive review of ion-exchange membrane transport has been completed recently by Verbrugge and Pintauro (1989).

Much of the early electrokinetic transport work was carried out by Dresner and Kraus (1963), Kobatake and Fujita (1964), and Osterle and coworkers (1965, 1968, 1971). Their theoretical transport models contained the Poisson-Boltzmann equation for the electric potential and ion concentration profiles in the radial pore direction, Nernst-Planck equations for the ion fluxes, and the Navier-Stokes equation for the axial fluid velocity in the membrane pore. The electric potential was written arbitrarily as the sum of radial and axial components, which allowed for a simplified one-dimensional solution to the Poisson-Boltzmann equation. The radial velocity was assumed to be zero everywhere in the pore, and pressure variations in only the axial pore direction were considered. Koh and Anderson (1975) and later Westermann-Clark and Anderson (1983) followed Osterle's modeling approach to simulate electrolyte transport through track-etched mica membranes. The transport models, however, were unable to match quantitatively the results of their electroosmosis and conductance experiments. Recently Cwirko and Carbonell (1989 and 1990) used the method of spatial averaging to model the transport of electrolytes in charged cylindrical pores. The model is applicable only for low pore wall charge, in which case the radial electric potential gradient near the pore wall is small.

The use of the Poisson-Boltzmann equation in electrokinetic transport models is based on the assumed ideal bulk-solution behavior of the solute and solvent. Electrokinetic models have recently been corrected to take into account finite ion size, an electric-field-dependent solvent dielectric constant, and ion hydration effects. Gur and coworkers (1978a, b), following Sparnaay's (1972) approach, modeled the distribution of ions in a charged capillary. An equation derived by Booth (1951) was used to describe variations of the solvent dielectric constant due to alignment of the water dipoles in the presence of an electric field, and the Boltzmann equation was altered to include a Born-model hydration-force correction term. The resulting modified Poisson-Boltzmann equation was used to show how ions of *identical* charge and *different* ionic radii yield different concentration, electric potential, and dielectric constant profiles within a capillary. Gur and Ravina (1978b, 1985), combined the modified Poisson-Boltzmann relationship with fluid-flow equations to model rheological electrokinetic phenomena in a rectangular capillary slit. More recently Pintauro and Verbrugge (1989) applied a modified Poisson-Boltzmann model to the equilibrium state of a cation-exchange membrane composed of cylindrical pores. Subsequent partition coefficient experiments with Nafion cation-exchange membranes and aqueous sulfuric acid solutions confirmed the accuracy of the equilibrium model (Verbrugge and Hill, 1988).

Experimental techniques to determine equilibrium absorption and transport rates in ion-exchange membranes have been developed in parallel with the formulation of new mathematical models. In particular the perfluorosulfonic acid (PSA) Nafion membranes have been investigated in detail due to their high chemical and mechanical stability and to their high ionic conductivity. Chandran et al. (1985), using electrochemical techniques, investigated ion absorption and electrodialysis transport behavior of Nafion 901 in concentrated NaOH. Similarly, Fioshin et al. (1986) studied dialysis and electrodialysis transfer of ions and water in a perfluorinated (MF-4SK) cation-exchange membrane using concentrated LiOH, NaOH, and KOH solutions. Wang et al. (1987), through spectrophotometric techniques, measured the diffusion of Co^{2+}, Cu^{2+}, and Cr^{3+} as a function of pH in Nafion 117. Lindheimer et al. (1987) used radiotracer methods to measure the absorption, self-diffusion, and electrodialysis transport of NaCl in Nafion 125. Using similar techniques Herrera and Yeager (1987) measured the absorption and self-diffusion of NaI, Na_2SO_4, and NaCl in sulfonated and carboxylated Nafion membranes. A series of papers describing various spectroscopic and radiotracer experimental techniques for absorption and transport under different driving forces, as applied to Nafion membranes, has been compiled by Eisenberg and Yeager (1982).

The purpose of this paper is to present the fundamental transport mathematical model for ion-exchange membranes. The models are an extension of the prior transport analysis of Gur et al. (1978a, b) for rectangular capillaries and the equilibrium work of Pintauro and Verbrugge (1989). Both ion solvation and an electric-field-dependent dielectric constant have been incorporated into the present analysis in order to simulate dialysis, electrodialysis, and reverse osmosis membrane separation processes. The models are used to simulate absorption of coions as well as the transport of coions and water for different alkali-metal sulfate solutions in a Nafion 117 cation-exchange membrane. The closely related alkali-metal cations (Li^+, Na^+, K^+, Rb^+, and Cs^+) were chosen for this study because they all have a noble-gas core; the low ionization potential of the alkali metals for their outermost electron dictates that the chemistry of these elements in aqueous environments is essentially that of $+1$, spherical cations. The chemistry of this group of elements is well understood and the radii of the spherical ions are tabulated in the literature.

Theory

The idealized ion-exchange membrane under consideration is assumed to consist of cylindrical pores of constant radius a with a uniform and continuous wall charge. The membrane, of thickness L separates two reservoirs containing aqueous electrolyte solutions of known concentration. Membrane permselectivity (Helfferich, 1962) results from: 1. the equilibrium partitioning of species at the pore-solution interfaces; and 2. solute and solvent transport through the membrane pores. The isothermal transport of species across the membrane is driven by a chemical or electrochemical potential gradient for neutral or ionic species, respectively, which leads to gradients in pressure, concentration, and electric potential within the membrane pores.

Steady-state transport is modeled for the case when the pressures and solute concentrations on either side of the membrane are known, and the applied current (or potential drop across the membrane) is specified. The Navier-Stokes equations for the radial and axial velocities and the equation of continuity for an incompressible fluid describe the convective movement of pore fluid (see, for example, the review by Verbrugge and Pintauro, 1989).

$$-\nabla p + \mu \nabla^2 v - \rho[\nabla \cdot vv] - \rho_e \nabla \phi = 0 \qquad (1)$$

$$\nabla \cdot v = 0 \qquad (2)$$

In these equations, p is the hydrostatic pressure, μ and ρ are the fluid viscosity and density, and v is the velocity vector. The electric potential ϕ within the pore is a function of both the axial and radial directions. The charge density of ions in the pore solution ρ_e is related to the molar concentration c of the m dissolved ions by

$$\rho_e = F \sum_{j=1}^{m} z_j c_j \qquad (3)$$

Nernst-Planck and material-balance equations (in the absence of homogeneous chemical reactions) describe the mass transfer of each dissolved species in the membrane pore

$$N_j = -z_j u_j F c_j \nabla \phi - \mathcal{D}_j \nabla c_j + c_j v \qquad (4)$$

$$\nabla \cdot N_j = 0 \qquad (5)$$

The right side of Eq. 4 contains specific terms for transport due to migration, diffusion, and convection, respectively.

The membrane pores investigated in this study are of very small diameter (≈ 60 Å), and the ionic flux expression in the radial direction can be replaced with an equilibrium relationship. This mathematical simplification arises because, for each ion, the radial flux $(N_j)_r$ and convective contribution to radial ion movement $(c_j v_r)$ are much smaller in magnitude than the diffusion and migration terms in Eq. 4. This equilibrium simplification allows us to write a modified Boltzmann expression for the radial distribution of ions, which is discussed below in the context of Eq. 10.

In Eq. 4 the free-solution diffusion coefficient of species j, $\mathcal{D}_j$, and the ionic mobility u_j are related to one another by the Nernst-Einstein equation, which is strictly applicable at infinite dilution (Newman, 1973)

$$\mathcal{D}_j = RTu_j \qquad (6)$$

Poisson's equation, with a variable dielectric constant ϵ relates the variation in the electric potential to the charge density of ions in the pore solution

$$\nabla \cdot (\epsilon \nabla \phi) = -\frac{\rho_e}{\epsilon} \qquad (7)$$

where ϵ is the permittivity of a vacuum (8.8542×10^{-12} C/V $\cdot$ m). High electrostatic fields in the radial pore direction can orient solvent (water) dipoles and reduce the polarizability and dielectric constant of the pore fluid, as compared to that in the external electrolyte. Booth (1951) derived a formula for the change in the dielectric constant with potential by taking into account the permanent dipoles and dipole-dipole interactions of the solvent species

$$\epsilon = n^2 + (\epsilon^o - n^2)\left(\frac{3}{\beta\nabla\phi}\right)\left[\coth(\beta\nabla\phi) - \frac{1}{\beta\nabla\phi}\right] \qquad (8)$$

where

$$\beta = \left(\frac{5\eta}{2kT}\right)(n^2 + 2) \qquad (9)$$

The constants n, η, and k are the optical refractive index, the dipole moment of the solvent molecule, and the Boltzmann constant, respectively. The value of the dielectric constant at the pore centerline is represented by ϵ^o. Because of the symmetric nature of the electric field about the pore centerline, ϵ^o is equal to the free-solution solvent dielectric constant.

The total potential of each ion is modified to include the standard electrostatic forces and forces due to ionic hydration (Gur et al., 1978b). Variations in the dielectric constant of pore solvent affect the hydration properties of the electrolyte. When the dielectric constant is treated as a local function of an ion's position in the pore, a modified form of the Boltzmann equation is obtained for the ion concentration profiles in the pore

$$c_j = c_j^o \exp\left\{\frac{-z_jF}{RT}(\phi - \phi^o) - \frac{A_j}{RT}\left(\frac{1}{\epsilon} - \frac{1}{\epsilon^o}\right)\right\} \qquad (10)$$

where ϕ^o is the electric potential at the pore centerline. The first exponential term describes electrostatic forces acting on the ions. The second term accounts for additional forces due to the existence of gradients in the dielectric constant, which Gur et al. (1978b) approximated with a Born hydration model. The hydration term can also be viewed as an activity coefficient for ionic species in the pore, as described by Hodgson (1970) in his analysis of reverse-osmosis cellulose acetate membranes.

The hydration constant A_j in Eq. 10 is a function of both the charge and size of the ionic species (Franks, 1973)

$$A_j = \frac{F^2 z_j^2}{8\pi\epsilon\mathcal{N}r_h} \qquad (11)$$

In Eq. 11, $\mathcal{N}$ is Avogadro's number and r_h is an ionic radius, which is equal to the sum of the Pauling crystallographic radius r_p and a solvation-sheath correction factor Δ (Franks, 1973)

$$r_h = r_P + \Delta \qquad (12)$$

The transport-model equations were solved in two dimensions. Such a two-dimensional numerical simulation is useful for structure/function transport models because it can be easily extended to analyze membranes with a variable pore diameter and a nonuniform wall-charge distribution. In addition, the electric potential was not decomposed arbitrarily into radial and axial components, as has been done previously to simplify the method of solution. [For examples, see Gross and Osterle (1968), Fair and Osterle (1971), and Koh and Anderson (1975)]. The axial gradients in the transport-model equations include a tortuosity term which takes into account the nonlinear path an ion must follow to pass through the membrane, as compared to the diffusion path in bulk electrolyte.

The following generalized, steady-state boundary conditions apply to a membrane separating two electrolyte solutions of known concentration; these conditions correspond to the experimental setup presented in the following section.

Axially at both pore/bulk-solution interfaces ($x = 0$ and $x = L$):

• A fully developed axial velocity profile was assumed

$$\frac{\partial v_x}{\partial x} = 0 \qquad (13)$$

• The radial concentration distribution of cations and anions within the pore at the pore/bulk-solution interfaces were set equal to the equilibrium absorption profiles, as proposed by Verbrugge and Pintauro (1989). The radial anion and cation concentration, electric potential, and solvent dielectric profiles at the interface were computed by solving Poisson's equation (Eq. 7), Booth's equation (Eq. 8), and the following modified Boltzmann relationship

$$c_j(r) = c_{\text{bulk}} \exp\left\{ \frac{-z_j F}{RT} \phi(r) - \frac{A_j}{RT}\left(\frac{1}{\epsilon} - \frac{1}{\epsilon^o}\right) \right\} \qquad (14)$$

When Eqs. 10 and 14 are combined to eliminate $c_j(r)$, the well known Donnan potential formula is obtained at the pore centerline

$$\phi^o = \frac{RT}{z_j F} \ln \frac{c_{\text{bulk}}}{c_j^o} \qquad (15)$$

The equilibrium concentration of anions (coions) in the membrane is related to the bulk external salt concentration by an ion partition coefficient. The partition coefficient K (with units of moles/cm³ wet membrane/moles/cm³ solution) is an experimentally measurable macroscopic solubility parameter, which is related to micro-level interactions within the pore. The ion concentration in a membrane pore is related to the bulk solution concentration at the pore-solution interface by (Verbrugge and Hill 1988)

$$K = \frac{\theta}{c_{\text{bulk}}} \frac{\int_0^a (c_j) 2\pi r\, dr}{\pi a^2} \qquad (16)$$

In this equation θ, the membrane porosity, converts the units of concentration from mole/cm³ of solution to mole/cm³ of wet membrane so that a direct comparison to experimental partition coefficient data can be made.

• The current density i in an electrolyte solution is generated by the motion of charged particles in the pore fluid,

$$i = F \sum_{j=1}^m z_j N_j \qquad (17)$$

The potential gradient at the pore entrance and exit is obtained by combining Eq. 17 with the molar-flux equation (Eq. 4)

$$\frac{\partial \phi}{\tau \partial x} = -\frac{i_x}{\kappa} - \frac{F}{\kappa} \sum_{j=1}^m z_j \mathcal{D}_j \frac{\partial c_j}{\tau \partial x} + \frac{F v_x}{\kappa} \sum_{j=1}^m z_j c_j \qquad (18)$$

In this equation τ is the membrane tortuosity factor and κ is the electrical conductivity of the pore electrolyte, which for dilute solutions is

$$\kappa = \frac{F^2}{RT} \sum_{j=1}^m z_j^2 \mathcal{D}_j c_j \qquad (19)$$

• The pressure at the upstream and downstream interfaces is known.

Radial symmetry at the pore centerline ($r = 0$) results in the following boundary conditions

$$\epsilon = \epsilon^o \qquad (20)$$

$$v_r = 0 \qquad (21)$$

$$\frac{\partial v_x}{\partial r} = 0 \qquad (22)$$

$$\frac{\partial p}{\partial r} = 0 \qquad (23)$$

$$\frac{\partial \phi}{\partial r} = 0 \qquad (24)$$

$$\frac{\partial (N_j)_x}{\partial r} = 0 \qquad (25)$$

The radial direction boundary conditions at the pore wall ($r = a$) are

$$v_r = 0 \qquad (26)$$

$$v_x = 0 \qquad (27)$$

$$(N_j)_x = 0 \qquad (28)$$

$$\frac{\partial \phi}{\partial r} = -\frac{\sigma}{\epsilon \epsilon} \qquad (29)$$

Equation 29 is Gauss's law, where σ is the charge density of fixed sites on the pore wall. The wall charge density σ and pore radius a are obtained from an assumed cylindrical pore geometry and from experimentally measured macroscopic dimensional (porosity) changes of the membrane (Verbrugge and Hill, 1988), as will be discussed in the following section.

The transport and electrokinetic equations presented above contain nine unknowns: pressure, electric potential, cation and anion concentrations, solvent dielectric constant, radial and axial velocities, and the anion and cation fluxes in the axial direction. Infinite dilution values were assigned to the solvent viscosity and density. The equilibrium partition coefficient of the anion species was matched to an experimentally-obtained anion partition coefficient by adjusting the cation solvation-sheath correction factor Δ (cf. Eq. 12). The diffusion coefficient of solvent (water) in the membrane pores was obtained from a series of radiotracer self-diffusion experiments with a Nafion cation-exchange membrane (to be discussed below). The anion and cation diffusion coefficients in the membrane were estimated from free solution diffusivity data (Newman, 1973). The membrane tortuosity was calculated from the ratio of anion diffusivities in free solution and in the membrane. Numerical

values for the refractive index and dipole moment of the solvent and crystallographic Pauling radii of ions were obtained from literature sources (Franks, 1973; Weast et al., 1980). There are no other adjustable parameters; the model as described is compared to equilibrium absorption and transport experiments without further adjustment of physicochemical parameters.

Experimental Studies

Five 0.1 M alkali-metal-cation sulfate solutions in Nafion 117 were investigated. Sulfur 35 (^{35}S) and tritium (T) were used to identify coion and water absorption and transport through the membrane. Nafion membranes are perfluorosulfonic acid membranes with a backbone consisting of tetrafluoroethylene units and side chains of the form $—O—CF_2—CF(CF_3)—O—CF_2—$ $CF_2—SO_3H$. The fixed-ion sites are provided by the hydrolyzed sulfonate group. The ionic strength within the membrane is quite high due to the high concentrations of fixed sulfonate groups in Nafion ($\approx$3M within the membrane pores) and the sulfate salts within the membrane pores are not fully dissociated, i.e.

$$M_2SO_4 \rightarrow M^+ + MSO_4^- \qquad (30)$$

where M refers to the alkali-metal species. No significant dissociation of MSO_4^-, however, takes place. This incomplete dissociation has been cited in Nafion membrane studies of Herrera and Yeager (1987) for Na_2SO_4 and Verbrugge and Hill (1988, 1990) for H_2SO_4.

A number of 1 in^2 (645 mm^2) diameter Nafion 117 films were prepared in a manner similar to that described previously by Verbrugge and Hill (1988). The membranes were boiled in concentrated nitric acid to remove impurities resulting from the fabrication processing of the membranes. Prior to each experiment, the membranes were refluxed in an alkali-metal sulfate solution of composition identical to that of the ensuing experiment and equilibrated in the same electrolyte at the temperature to be used in the experiment (20°C).

Equilibrium experiments

Uptake Analysis. After the films were conditioned in their corresponding electrolyte solution, three disc samples were placed together in a vial containing 10 ml of fresh alkali-metal sulfate solution. 11.3 μCi of T and 5.3 μCi of ^{35}S were then added to each vial. After 24 hours, a 0.1 mL aliquot of the tagged solution was transferred into a counting vial containing 15 mL of liquid scintillation solution (Aqua Mix, ICN Radiochemicals, Inc.) for analysis of T and ^{35}S which are beta-ray emitters and are efficiently measured by liquid scintillation spectrometry. T and ^{35}S concentrations were measured simultaneously to ensure that the same conditions exist for each species at the time of measurement. For each alkali-metal sulfate, the three disc samples were removed from the tagged acid solution and blotted with filter paper to remove any excess solution from the surface of the discs. Each disc was placed in a counting vial containing 15 mL of liquid scintillation liquid. After 24 hours the total moles of sulfate anions and water which leached out of the membrane were determined (Verbrugge and Hill, 1988).

Porosity Experiments. The porosity of Nafion was determined by measuring the macroscopic swelling of the membrane when it is equilibrated in a given salt solution. After the disc samples were conditioned in a given salt solution, they were blotted dry of any excess surface solution and the thickness and diameter were measured. The samples were then heated in an oven at 100°C for four hours to evaporate the water from each membrane sample, and the thickness and diameter were measured again. A constant-load thickness gauge (Sterlinger Company) was used to measure the membrane thicknesses. The discs were placed between glass slides, and the membrane diameters were measured using an optical microscope.

Transport experiments

Radiotracer dialysis and electrodialysis experiments were carried out in the cell shown in Figure 1, which was constructed of 1 cm thick Lucite and contained sampling ports and a channel for electrolyte transport. The transport channel had a cross-sectional area of 0.785 cm^2. The cell was sealed during each experiment except while aliquots were being removed. After assembly of the cell, the test electrolytes were added to the reservoirs; radiotracer species were then added to one of the compartments, henceforth referred to as the hot reservoir. The cold-side chamber initially contained no tritiated water. A 1 mL aliquot of tritiated water was added to the hot-side compartment. (The initial hot-side THO concentration was 1.6 $\times$ 10^{14} atoms/mL. The initial ^{35}S concentration in the hot reservoir was known precisely, and ranged between 5.96 $\times$ 10^{12} and 2.64 $\times$ 10^{12} atoms/mL for the various experiments.) Teflon-coated magnetic stirrers were employed in each reservoir to mix the electrolyte during the course of an experiment. Each reservoir contained a platinum electrode so that the effect of an applied constant current on membrane water transport could be measured during a series of electrodialysis experiments. The effective diffusion coefficients of water and coion were obtained from a single dialysis experiment.

Electrodialysis experiments were conducted first. The electrode in the hot reservoir was made the anode. The overall reactions at the electrodes are as follows:

$$\text{Anode:} \quad 2H_2O \rightarrow 4H^+ + O_2 + 4e^- \qquad (31)$$

$$\text{Cathode:} \quad 4H^+ + 4e^- \rightarrow 2H_2 \qquad (32)$$
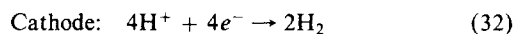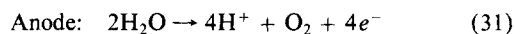
The current passed between the electrodes was controlled by a Princeton Applied Research Model 273 potentiostat/gal-
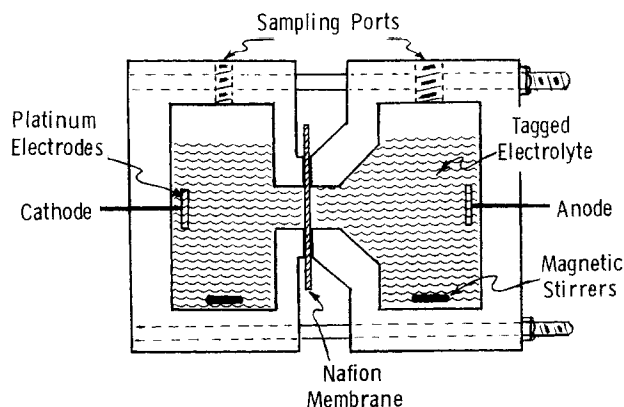

Figure 1. Radiotracer cell.

vanostat. The duration of an electrodialysis experiment varied from 75 minutes for a 1 mA current level (1.27 mA/cm²) to 10 minutes for 400 mA (510 mA/cm²). These time durations were selected so that small, but approximately equal, amounts of electrolyte were transported from the hot to the cold chamber. Aliquots of 100 μL were withdrawn from the cold side at five time intervals equally space over the duration of an experiment for each constant current applied. Only water fluxes through the membrane were measured in these experiments. Figure 2 shows plots of the cold-side concentration of THO vs. time for different current densities.

At the conclusion of an electrodialysis experiment, the cold-side T and ³⁵S concentrations were recorded and, in the absence of current, the diffusion experiments were initiated. The duration of each diffusion experiment was nominally 3 days to ensure that at least 0.1% of the radioactivity in the hot reservoir was transported to the cold chamber, providing a relative error of the radiometric analysis of less than 2% (Verbrugge and Hill, 1988). This precision coupled with five concentration determinations over the course of an experiment provided adequate information for determining the transport characteristics of the alkali-metal-salt/Nafion system. The diffusion coefficients of the five different alkali-metal-sulfate anions and of water were obtained from these experiments. The ratio $(c_{MSO_4}^{COLD})/(c_{MSO_4}^{HOT})$ is plotted as a function of time in Figure 3. The slope of each line is related to the respective alkali-metal sulfate diffusion coefficient (as will be discussed below). The water diffusivity was obtained from the tritiated-water diffusion across the membrane. Since there was a significant amount of tritium in the cold side at the start of a diffusion experiment, longer time intervals were required between aliquot withdraws (relative to the sulfate-diffusion experiments) to maintain high sensitivity. The increase in cold-side THO concentration with time for the five alkali-metal sulfate salts is shown in Figure 4.

Results and Discussion

Equilibrium Experiments. The effective porosity of the perfluorosulfonic acid membranes is defined as

$$\theta = \frac{V_{wet} - V_{dry}}{V_{wet}} \qquad (33)$$
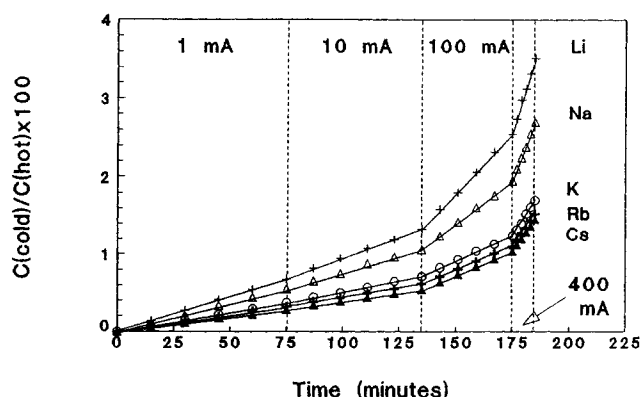
Figure 2. Cold-side concentrations of tritiated water THO vs. time for the electrodialysis experiments.

The superficial area for transport was 0.785 cm². 0.1M alkali-metal-sulfate solutions were employed in each reservoir. The cell currents for the various time intervals are listed.
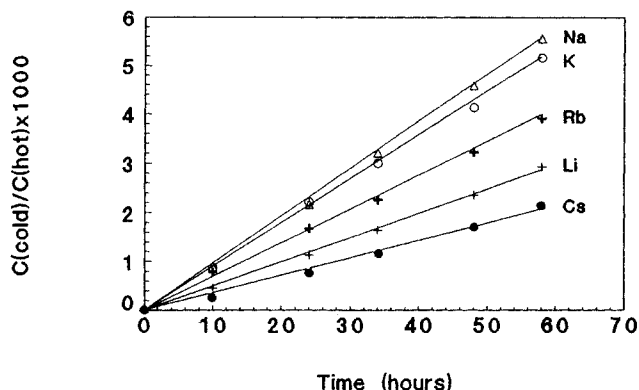
Figure 3. Cold-side concentration of M³⁵SO₄⁻ species vs. time.

M refers to the alkali-metal atom. The different alkali-metal atoms used in the 0.1M alkali-metal sulfate solutions are listed. The symbols represent experimental results.

where V_{wet} is the volume occupied by the membrane when it is equilibrated with an electrolyte solution, and V_{dry} is the volume of the dry membrane. The term *effective* porosity has been used since the poly(tetrafluoroethylene) backbone of the Nafion films is probably not rigid, and it may not have the same density in the dry state as in the fully hydrated state. In actuality, θ is a relative, fractional volume change upon membrane hydration. The concept of porosity in ion-exchange membranes with $\approx$50-Å pore dimensions, as seen in x-ray scattering experiments (Gierke, 1977), is not well-defined. As Helfferich (1962) points out, some of the water is bound to the coordination spheres of the fixed sulfonate sites as well as those of the mobile coions and counterions, and some fraction of the water is free for more facile transport. The application of the term porosity or fractional volume change, however, has proven useful for the explanation of transport in ion-exchange membranes, and it will be used in our analysis. The cylindrical pore radius, which appears in the electrokinetic transport model, is determined from (Verbrugge and Hill, 1988)

$$a = a_{H_2O} \frac{d}{d_{H_2O}} \sqrt{\frac{\theta}{\theta_{H_2O}}} \qquad (34)$$

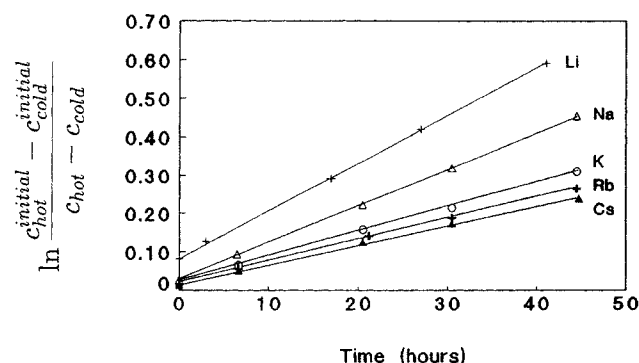where the subscript H₂O refers to a membrane boiled and

Figure 4. Concentration function of the tritiated-water species THO vs. time for various 0.1M alkali-metal sulfate reservoir concentrations.

equilibrated in a pure water reservoir, and d is the diameter of a membrane disc that is equilibrated with the test electrolyte. The surface charge density is related to the membrane porosity and pore radius by

$$\sigma = \frac{\rho_{dry}(1 - \theta)aF}{2\theta \left(\dfrac{1,000}{IEC}\right)} \qquad (35)$$

In Eq. 35, IEC is the membrane ion-exchange capacity (with units mequiv/g), which relates the number of fixed charges to the specific weight of membrane polymer. Experimental membrane porosities and film thicknesses as well as computed pore radii and pore wall charge densities for Nafion 117 are listed in Table 1 for five alkali metal sulfate salts at 0.1 M concentration. The computed pore radii agree well with those reported by Gierke and Hsu (1982) (25-50 Å) for Nafion membranes boiled in a 0.2% NaOH solution.

The porosity results of Table 1 illustrate clearly the effect of the alkali-metal ion radii on membrane porosity. The unsolvated radii for the alkali-metal ions are presented in Table 2. The smaller Li^+ cation is more strongly hydrated, leading to larger water contents within the membrane. In addition, it is well established for cation-exchange resins that the order of preference for alkali-metal cation association with the fixed anion site is $Li^+ < Na^+ < K^+ < Rb^+ < Cs^+$ (Cotton and Wilkinson, 1972). When the cesium cation, for example, associates with a fixed sulfonate site in Nafion, some of the cesium's and sulfonate's hydration sheaths are lost; hence it follows that ions which are more strongly hydrated and associate less with the fixed-charge sites yield larger membrane water contents and porosities. For the alkali-metal-cation series, our porosity results can be summarized as:

DECREASING POROSITY →

$$\theta : Li^+ > Na^+ > K^+ > Rb^+ > Cs^+$$

The actual number of water molecules in the membrane was obtained quantitatively from the equilibrium uptake experiments. Figure 5 shows membrane water concentrations in the form of a water partition coefficient, K_{H_2O}, where

$$K_{H_2O} = \frac{c_{H_2O}^{membrane}}{c_{H_2O}^{reservoir}} \qquad (36)$$

It is obvious that the membrane porosity data and the membrane water-concentration data are quite similar, as should be

Table 2. Unsolvated Ion Radii (Noyes, 1962, 1964)

Cation	Ionic Radii, Å
Li^+	0.60
Na^+	0.95
K^+	1.33
Rb^+	1.48
Cs^+	1.69

the case since the pore fluid in the membrane is composed predominantly of water molecules. If the density of water within the membrane were unity, then the ratio K_{H_2O}/θ would be unity since the concentration of water within the membrane pores would essentially equal that of the reservoir. (The additional volume occupied by the 0.1 M alkali-metal salt is a second-order effect.) For the lithium sulfate case, $K_{H_2O}/\theta \approx 1$. This ratio increases throughout the rest of the alkali-metal series to ≈ 2 for 0.1 M cesium sulfate. We can infer from these results that lithium cations are so strongly hydrated that the water concentration within the membrane is identical to that of the adjacent reservoirs. Conversely, the less-solvated alkali-metal ions yield lower membrane water contents, and structure-forming mechanisms in the pore fluid result in increased water densities within the membrane. Structuring in the aqueous pore fluid could result from the electrostatic field across the pore that is generated by the fixed sulfonate charges and tends to align the dipole-containing water molecules. Lower porosities would be expected to produce more structuring since the pore walls containing the charged sulfonate sites would be closer together (assuming the reduced porosities translate into decreased membrane pore radii).

The radiotracer salt uptake data are shown in Figure 6. The ordinate in this figure is the salt partition coefficient, which is the salt concentration in the membrane divided by the reservoir salt concentration.

$$K_{salt} = \frac{c_{salt}^{membrane}}{c_{salt}^{reservoir}} \qquad (37)$$

The salt partition coefficient appears in the electrokinetic transport model as the concentration boundary condiiion at the pore/bulk-solution interface. There are two competing effects that can be identified for the explanation of the data in Figure 6. The first effect is more obvious; the porosity data of Table 1, considered independently, would dictate that the salt partition coefficient should be highest for lithium and decrease throughout the rest of the alkali-metal series. The second effect results

Table 1. Membrane Porosity, Membrane Thickness, Pore Radius, and Wall Charge for 0.1 M Alkali Metal Sulfates in Nafion 117

Electrolyte	Membrane Porosity	Membrane* Thickness (μm)	Pore Radius (Å)	Wall Charge (C/m²)
Li_2SO_4	0.312	258	32.29	−0.547
Na_2SO_4	0.260	252	29.40	−0.676
K_2SO_4	0.210	242	26.50	−0.803
Rb_2SO_4	0.185	240	24.80	−0.883
Cs_2SO_4	0.178	233	24.40	−0.908

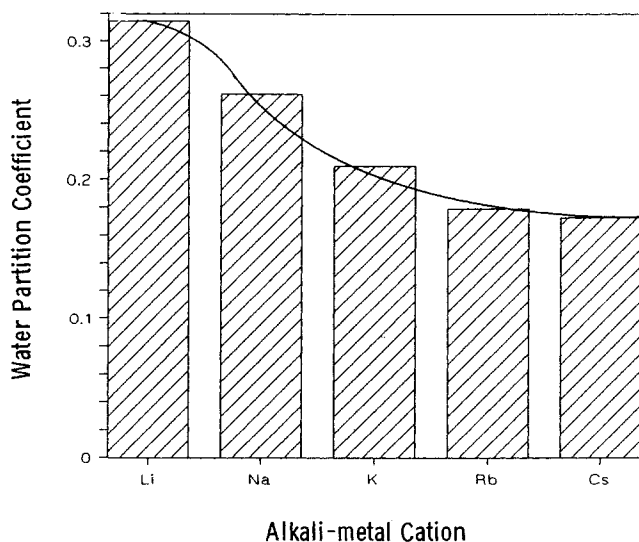*A dry membrane thickness of 210 ± 3 μm was measured for each membrane.

Figure 5. Water partition coeficient of perfluorosulfonic-acid membranes equilibrated with 0.1M alkali-metal sulfate solutions.

from the solvation forces within the membrane. For equivalent pore radii, larger electric fields are generated across the membrane pores by species that are more strongly hydrated. Briefly stated, the more strongly hydrated counterions (of $+1$ charge) are not allowed to approach closely the sulfonate fixed-charge sites (of -1 charge) due to their larger hydration sheaths—this results in a separation of charge. Larger separations of charge generate stronger electric fields across the membrane pores, which in turn repel coions from entering the pores and yield lower salt partition coefficients. These two effects can be summarized as follows:

DECREASING K_{SALT} →

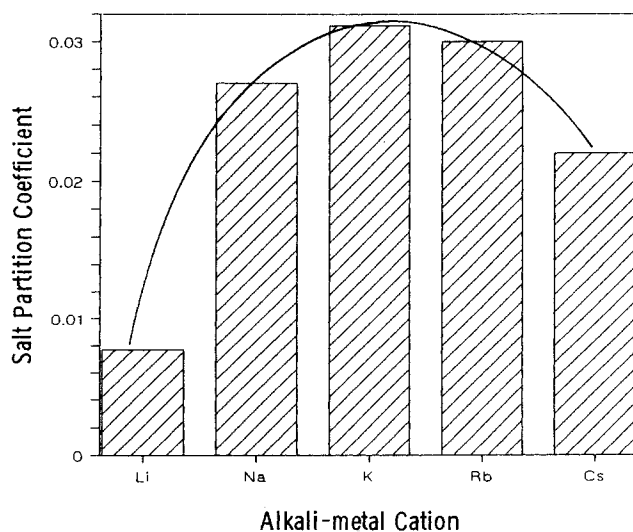Porosity effect on K_{SALT}: $Li^+ > Na^+ > K^+ > Rb^+ > Cs^+$

Figure 6. Salt partition coefficient of perfluorosulfonic-acid membranes equilibrated with 0.1M alkali-metal sulfate solutions.

Hydration (Field) effect on K_{SALT}:

INCREASING K_{SALT} →

$Li^+ < Na^+ < K^+ < Rb^+ < Cs^+$

These two effects manifest themselves in the creation of a maximum in the salt-partition coefficient data shown in Figure 6.

Transport Experiments. Radiotracer self-diffusion experiments for water and anions allow for two important simplifications: 1. only a fraction of a percent of the hot-side radionuclide need be transferred to the cold side reservoir to ensure high precision; and 2. the system is not altered by the presence of radiotracer species (i.e., no porosity changes, no potential-gradient changes, and no convection). Under these conditions the cold-side concentration $c_{MSO_4^-}^{COLD}$ of the radiotracer species at any time t can be expressed as

$$(c_{MSO_4^-}^{COLD}) = \frac{(D_{MSO_4^-})(K_{MSO_4^-})(c_{MSO_4^-}^{HOT})S}{LV} t \quad (38)$$

where D_{MSO_4} denotes the membrane diffusion coefficient of the sulfate radiotracer species, L is the membrane thickness, S is the superficial area of membrane normal to the direction of transport, and V is the volume of the chamber on either side of the membrane. A closer inspection of the assumptions inherent in writing this equation for self-diffusion or neutral-molecule diffusion through a membrane from one reservoir to another has been published recently (Verbrugge, 1989). At the beginnning of the THO dialysis experiments, there was a small amount of tritium in the cold-side compartment since the electrodialysis experiments were conducted first. In this case, the water diffusion coefficient was computed using the following equation,

$$\ln \frac{(c_{THO}^{COLD} - c_{THO}^{HOT})|_{initial}}{c_{THO}^{COLD} - c_{THO}^{HOT}} = \frac{2K_{THO}D_{THO}S}{LV} t \quad (39)$$

Experimentally determined diffusion coefficients of water and sulfate ions are plotted in Figure 7 for the various alkali-metal
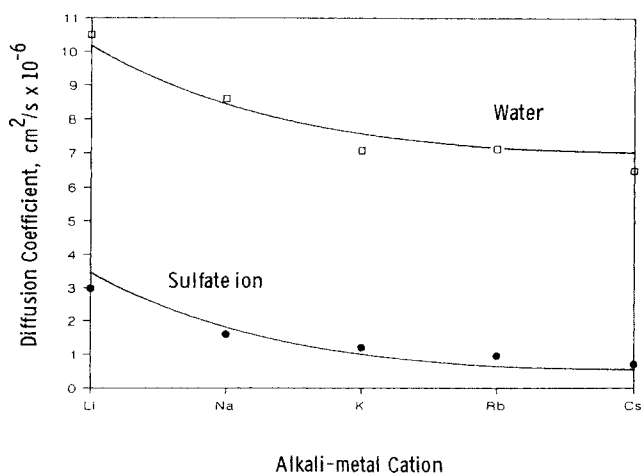

Figure 7. Water-molecule and sulfate-ion diffusion coefficients for various 0.1M alkali-metal sulfate reservoir concentrations.

sulfate salts. A notable feature of this plot is the similar trend for the water and sulfate-ion diffusivities. The experimental anion diffusion coefficients are related to the corresponding free-solution coefficients $\mathcal{D}$ by (Tuwiner, 1962; Epstein, 1989)

$$D = \frac{\mathcal{D}}{\tau} \tag{40}$$

where τ is a membrane tortuosity factor. The free solution diffusion coefficient of bisulfate anions at infinite dilution is independent of the cation species and is related to equivalent ionic conductance λ data (Newman, 1973; Franks, 1973) by

$$\mathcal{D}_j = \frac{RT\lambda_j}{|z_j|F^2} \tag{41}$$

Table 3 lists membrane tortuosity factors computed from the experimental anion diffusion coefficient data and Eqs. 40 and 41.

For Nafion membranes containing aqueous electrolytes, a Bruggeman-type relationship (Bruggeman, 1935) has proven useful in correlating the tortuosity factor and the membrane porosity (Yeo and Chin, 1980; Yeo, 1983; Verbrugge and Hill, 1990)

$$\tau \sim e^{-B\theta} \tag{42}$$

where B is a constant characteristic of the membrane/electrolyte system. The slight dependence of the experimental water and sulfate-ion diffusion coefficients on the type of alkali cation can be explained in terms of the membrane porosity data shown in Table 1 or the tortuosity factors in Table 3. Since the membrane porosity decreases from a value of 0.312 for Li to a value of 0.178 for Cs (c.f. Table 1), tortuosities given by Eq. 42 (or listed in Table 3) follow the trend:

DECREASING TORTUOSITY →

$$\tau : Cs^+ > Rb^+ > K^+ > Na^+ > Li^+$$

which explains the similar shape of the effective diffusion coefficient curves in Figure 7.

Mathematical Model

The two-dimensional electrokinetic mathematical model has been solved on an IBM 3081 mainframe computer using the implicit alternating-direction finite-difference technique (Carnahan et al., 1969; Lapidus and Pinder, 1982), with constant mesh point spacing in the axial direction and variable mesh point spacing in the radial direction. The model was used to simulate radioactive isotope absorption, self-diffusion, and electrodialysis

experiments (Lakshminarayanaiah, 1969a). To test the mathematical models, computed partition coefficients and ionic fluxes were compared with experimentally obtained radiotracer equilibrium and transport data.

The solvation-sheath correction factor for the anion species (Δ in Eq. 12) was fixed at 0.1 Å. In order to determine the hydration parameter for cations in a Nafion membrane pore, experimental and theoretical anion partition coefficients were matched. A computer optimization technique was used to find the cation value of Δ, which reproduced experimentally determined partition-coefficient data, as defined by Eq. 16. The existence of a single optimum value of Δ was tested by starting the optimization technique with different initial guesses for the hydrated radius. Theoretically computed partition coefficients were found to be strongly dependent on the cation hydration parameter and relatively insensitive to that of the anion. Table 4 lists the experimental anion partition coefficients and the optimized Δ values for all alkali metal cations. The error between the experimental and optimized partition coefficients was less than 0.5% for all electrolytes examined.

The Δ values in Table 4 are different for each alkali metal cation. Latimer et al. (1939) suggested originally that $\Delta = 0.85$ Å for all the alkali metal cations in free solutions. Subsequently Powell and Latimer (1951), Noyes (1962), and Stokes (1964) reported values of 2.00, 0.43, and 2.8 Å, respectively, for all alkali metal cations. As evidenced by the conflicting literature values, Δ must be regarded as an adjustable parameter in the model. Additional work in this area is required to elucidate the precise meaning of this hydration parameter.

Pore profiles for the electric potential, solvent dielectric constant, cation and anion concentrations, pressure, and velocities were calculated using the values of Δ obtained in the equilibrium analysis. The presence of radiotracer species (T and ^{35}S) was ignored in the computation of these profiles because they were always present in concentrations at least six orders of magnitude smaller than the nontracer electrolyte. The concentration and molar flux of the radiotracer species were calculated once the electric potential, dielectric constant, and fluid velocity were known. The concentration of radiotracer at the upstream end of the pore was always specified; at the downstream pore location, the concentration of radiotracer was set equal to zero.

The computed variation in solvent dielectric constant is shown in Figure 8. At the pore centerline, the dielectric constant is 78, identical to that for bulk water. Near the wall, the dielectric constant decreases significantly due to alignment of the water dipoles by the electric field. This low dielectric constant indicates that the water molecules are *frozen* in position adjacent to the pore wall, as has been speculated from spectroscopic membrane measurements of water in Nafion and cellulose

Table 3. Tortuosities for 0.1 M Alkali Metal Sulfates in Nafion 117

Electrolyte	Tortuosity Factor
Li_2SO_4	4.430
Na_2SO_4	8.417
K_2SO_4	10.23
Rb_2SO_4	12.09
Cs_2SO_4	16.62

Table 4. Anion Partition Coefficient and Optimized Cation Solvation Sheath Thickness for 0.1 M Alkali Metal Sulfates in Nafion 117

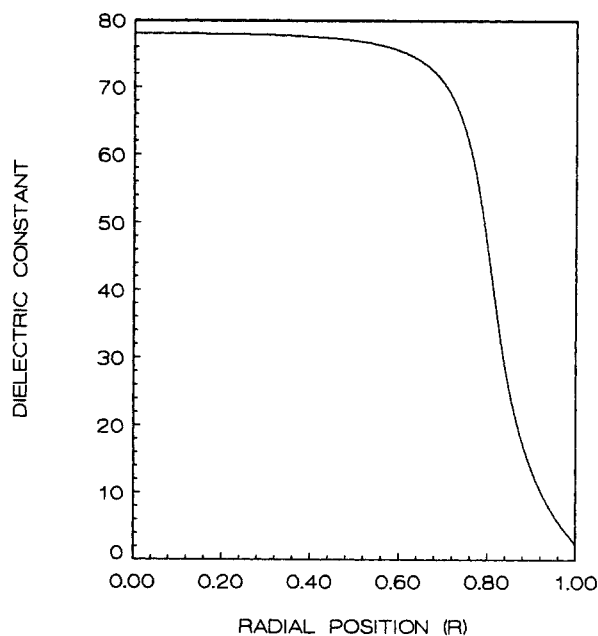| Electrolyte	K_{anion}	Δ_{cation}(Å)
Li_2SO_4	0.0078	0.202
Na_2SO_4	0.0270	0.927
K_2SO_4	0.0310	3.239
Rb_2SO_4	0.0300	9.545
Cs_2SO_4	0.0220	2.650

Figure 8. Solvent dielectric-constant profile for 0.1 M Na₂SO₄ in Nafion 117.

No axial variations are observed because of equilibrium. Radial coordinate: $R = r/a$.

variations in the dielectric constant are considered in the model, no significant variations in the predicted potential profile are observed relative to traditional electrokinetic membrane models with an invariant dielectric constant. The incorporation of hydration forces, however, substantially changes the predicted potential profile. The same result was observed by Pintauro and Verbrugge (1989) with their equilibrium model for ion-exchange membranes. The present model predicts high electro-static fields and large coion exclusion in pores of ≈ 60 Å diameter. In order to explain the observed coion rejection in Nafion membranes using traditional electrokinetic theories, pore radii as small as 5-8 Å have been employed (Capeci et al., 1989). Our results also call into question the proposed *cluster-network* pore model of Nafion (Gierke, 1982). This structure, consisting of large (50 Å) inverted micelles interconnected by narrow (10 Å diameter) capillaries, has been used previously to explain the high absorption and low transport rates of coions in Nafion.

Figure 10 shows the coion (NaSO₄⁻) concentration profile in a Nafion pore. Electrostatic repulsion prevents the coions from approaching the pore wall. At the pore centerline the coion concentration is lower than that in the bulk electrolyte, due to a nonzero electric potential at the center of the pore.

The computed counterion (Na⁺) concentration in a Nafion pore is shown in Figure 11. The counterion concentration at the pore centerline is greater than that in the bulk electrolyte because of the nonzero electric potential. A local maximum is observed for the counterion concentration near the pore wall because hydration effects dominate over electrostatic field effects at this location. Close to the pore wall, electrostatic attraction prevails, and larger counterion concentrations are observed. To explain the unusually high concentration at the pore wall, it is helpful to consider the corresponding fixed-charge

acetate membranes. (See, for example, Escoubes and Pineri (1982) and Scherer and Bailey (1983).

The predicted electric-potential profile is plotted in Figure 9. A large electric-potential difference between the pore centerline and the pore wall is predicted because of the inclusion of ion hydration and variable dielectric constant effects. When only
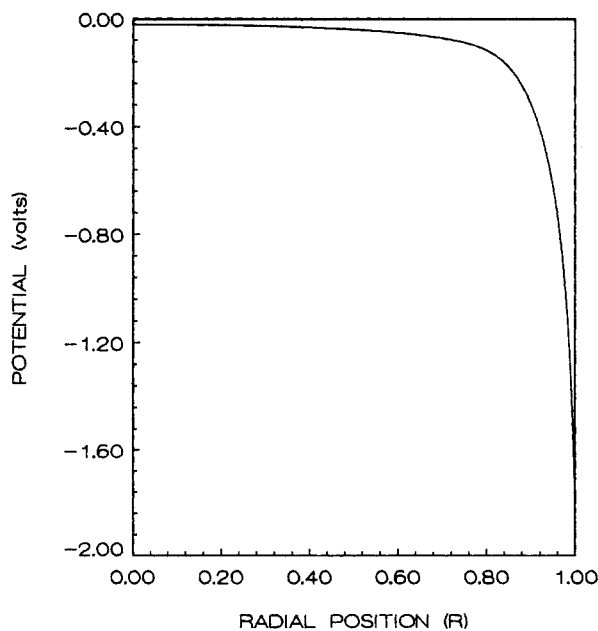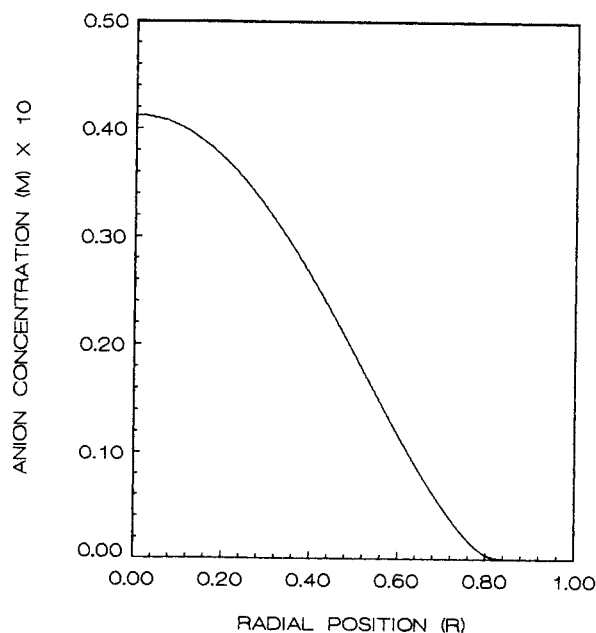

Figure 9. Electric-potential profile for 0.1 M Na₂SO₄ in Nafion 117.

Radial coordinate: $R = r/a$.

Figure 10. Anion-concentration profile for 0.1 M Na₂SO₄ in Nafion 117.
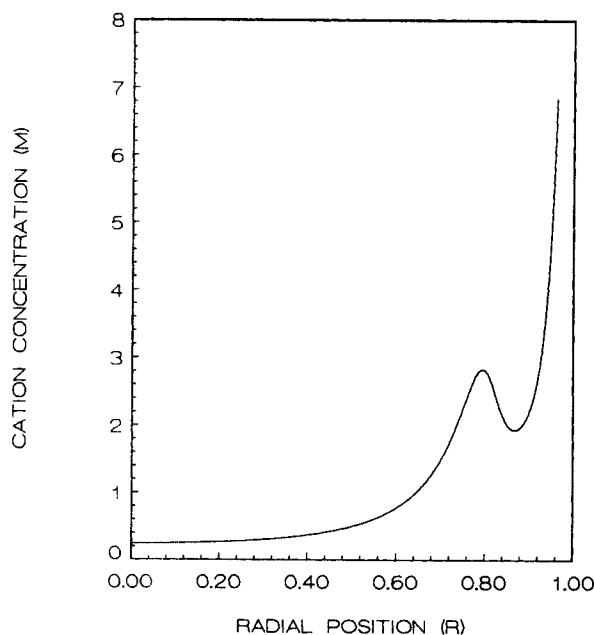
Radial coordinate: $R = r/a$.

Figure 11. Cation-concentration profile for 0.1 M Na₂SO₄ in Nafion 117.

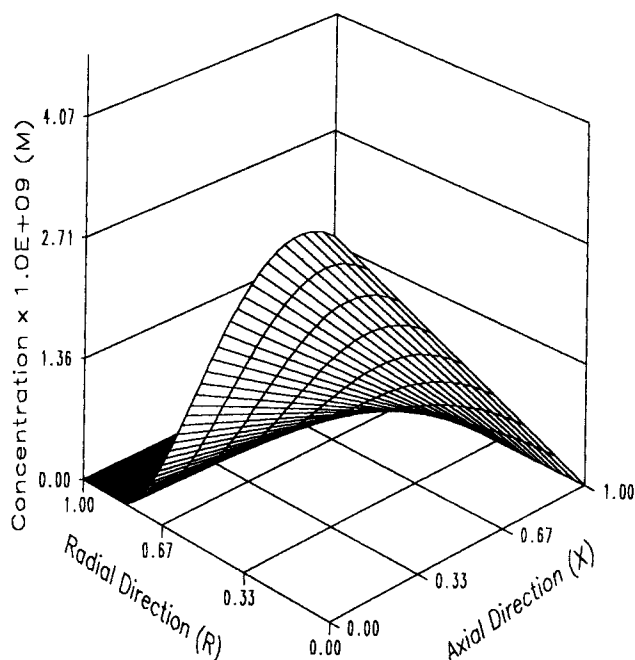Radial coordinate: $R = r/a$.

Figure 12. Radiotracer Na³⁵SO₄⁻ concentration profile for 0.1 M Na₂SO₄ in Nafion 117.

Radial coordinate. $R = r/a$; axial coordinate: $X = x/L$.

concentration (c_{fixed}). If the fixed-charge groups have an ionic diameter (d_{fixed}) of 3 Å, c_{fixed} can be estimated as

$$c_{fixed} = \frac{\sigma}{Fd_{fixed}} \quad (43)$$

from which one calculates c_{fixed} to be approximately 21 M for the sodium sulfate case. It should be noted, when viewing the results in Figure 11, that ionic concentrations at a distance less than the hydrated counterion radius from the pore surface are not physically meaningful.

The predicted concentration profile for the Na³⁵SO₄⁻ tracer species is shown in Figure 12. A concentration gradient of the tracer species is established across the membrane, causing the tracer to diffuse from the upstream to the downstream reservoir. The simulated and experimental anion-tracer fluxes for alkali metal sulfate salts are compared in Figure 3. The solid lines in this figure represent the simulation results. The downstream tracer concentration is normalized with respect to that in the upstream compartment, which remains essentially constant with time. Excellent agreement with experimental results is obtained for all the alkali metal sulfates. The largest difference between theory and experiment, of 1.2%, was for the lithium sulfate radiotracer; for the other salts the difference ranged between 0.655 and 0.991%.

Figure 13 shows the predicted increase in downstream tracer concentration with time for diffusion models which use either the traditional or the modified Poisson-Boltzmann equation. When the membrane transport model is solved with the traditional Poisson-Boltzmann equation (i.e., an invariant dielectric constant and no hydration effects), the electric-potential difference between the pore centerline and the pore wall is small. As a result, coion exclusion is underestimated and high anion ra-

diotracer molar fluxes are computed. The overestimation in the tracer molar flux was highest for lithium sulfate (30%) and lowest for rubidium and cesium sulfates (6%). The use of the modified Poisson-Boltzmann equation in the model shows excellent agreement between theory and experiment.
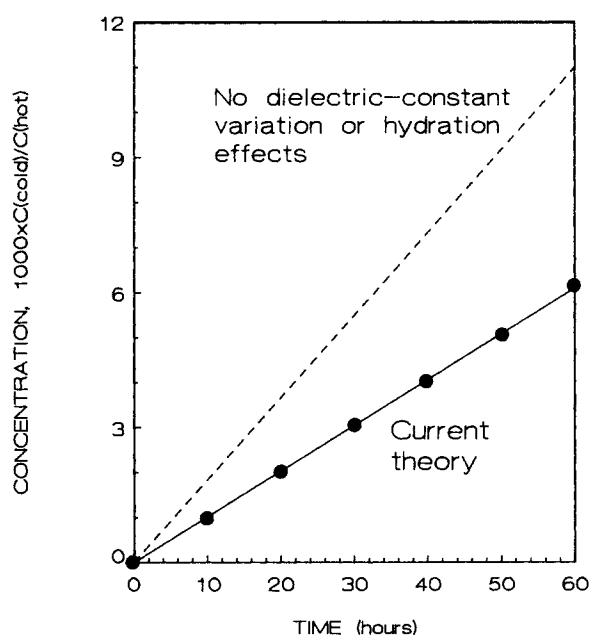

Figure 13. Molar fluxes for sodium sulfate tracer at a total 0.1 M concentration.

Modified Poisson-Boltzmann equation (solid line), and the traditional Poisson-Boltzmann equation (broken line). The circles denote experimental results.

In addition to the self-diffusion tracer experiments for the 0.1 M alkali-metal sulfate solutions, water transport has also been simulated. The driving force across the membrane was an applied constant electric current of either 1, 10, 100, or 400 mA. [Earlier work in this area can be examined by inspection of References 12–48 of Lakshminarayanaiah's paper (1969b).] During electrodialysis the THO molecules are transported across the membrane by diffusion as well as by bulk convection due to an electroosmotic flow generated by the cell current. The average molar flux of tritiated water through a membrane pore was calculated in the following manner. The equation of continuity ($\nabla \cdot N_o = 0$) was solved using the appropriate radial and axial molar flux equations and boundary conditions. The radial molar flux of water is given by

$$(N_o)_r = -D_o \frac{\partial c_o}{\partial r} + c_o v_r \qquad (44)$$

The convective term in this equation is insignificant (v_r is of the order 1.0×10^{-20} m/s), and $c_o v_r$ can be discarded. To find the radial distribution of water within the pore, a relationship between the concentration of ions in solution and the water concentration is needed. Since such a relationship was not known, an average radial concentration of tritiated water within the pore was used, as determined from experimental water partition coefficients. In general, it is expected that radial variations in the water concentrations are very small and only axial concentration gradients need be considered for the transport of tritiated water through a membrane pore

$$(N_o)_x = -\frac{\mathcal{D}_o}{\tau} \frac{\partial c_o}{\partial x} + c_o v_x \qquad (45)$$

where the quantity $(\mathcal{D}_o/\tau)$ is the experimentally determined water diffusion coefficient. At the upstream end of the pore ($x = 0$) the tritium concentration is constant and known,

$$c_o = c_{THO} \qquad (46)$$

and at the downstream end of the pore ($x = L$)

$$c_o = 0 \qquad (47)$$

The velocity v_x is a function of the electric potential gradient, as indicated by Eq. 1. The diffusion coefficient term for water ($\mathcal{D}_o/\tau$) is dependent on the nature of the cation and anion species in the membrane (cf. Figure 7).

Figure 14 compares the simulated and experimental electrodialysis water fluxes for Na_2SO_4 and K_2SO_4 solutions at an external concentration of 0.1 M. The same behavior was obtained for the other alkali-metal solutions. An analysis of the magnitude of the two terms on the righthand side of Eq. 45 indicated that at 1 and 10 mA, water transport is due mainly to THO diffusion through the pore, whereas at 100 and 400 mA the electroosmotic convection term dominates. Although the numerical results qualitatively agree with experiments, a lower water flow rate is predicted at the highest current: i.e., the model underestimates electroosmotic velocities at 400 mA. The discrepancy between theory and experiment for the 400 mA results cannot be explained at the present time. Possible explanations are that the assumption of equilibrium at the membrane/
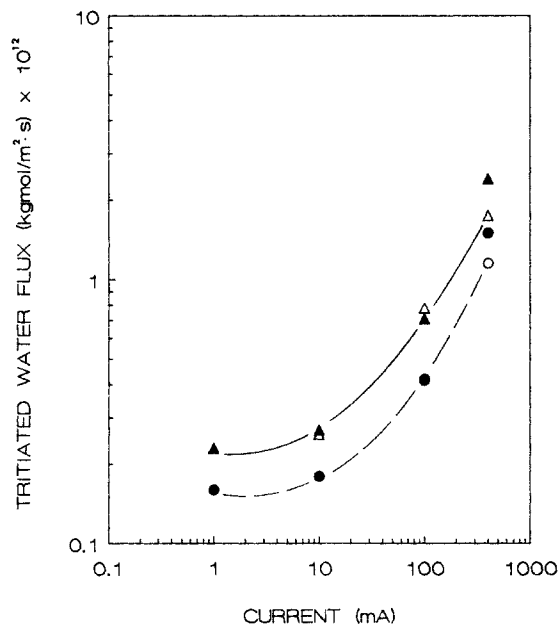

Figure 14. Simulated and experimental tritiated water molar fluxes for Na_2SO_4 and K_2SO_4 solutions at a concentration of 0.1 M as a function of current density.

The cross-sectional area for transport was 0.785 cm². Experimental (▲ : Na, ● : K) and theoretical (△ : Na, ○ : K). The lines were drawn through the theoretical points to represent the model predictions.

solution interface is not valid for high currents and/or the membrane is undergoing morphological changes under high-current conditions [as suggested by Lakshminarayanaiah (1969a, p. 256)].

The computed velocity profile for an electroosmotic process is shown in Figure 15 when the electrolyte is 0.1 M Na_2SO_4 and the applied current is 400 mA. The simulated velocity differs significantly from a Poiseuille velocity profile, which has been used in some electrokinetic transport models (see for example Walton and White, 1987).

Conclusions

A two-dimensional, molecular-level electrokinetic mathematical model is developed for solute absorption and solute and solvent transport in an ion-exchange membrane composed of cylindrical pores. The model includes ionic hydration, solvent dipole-dipole interactions, and alignment of solvent dipoles by an electric field induced by the fixed charges on the pore wall. The membrane pore radius, pore-wall charge density, and a solvation-sheath correction factor for both cations and anions need to be specified for a complete solution of the mathematical equations. These parameters are computed from experimentally-obtained equilibrium absorption data for five different 0.1 M alkali-metal sulfate solutions in a Nafion 117 cation-exchange membrane. To solve the transport equations for a given solute/ solvent/membrane system, the diffusion coefficients of solvent, coion, and counterion must also be specified. The diffusivity of water is obtained from self-diffusion radiotracer transport experiments; the coion and counterion diffusivities are computed from free-solution equivalent conductance data. Membrane
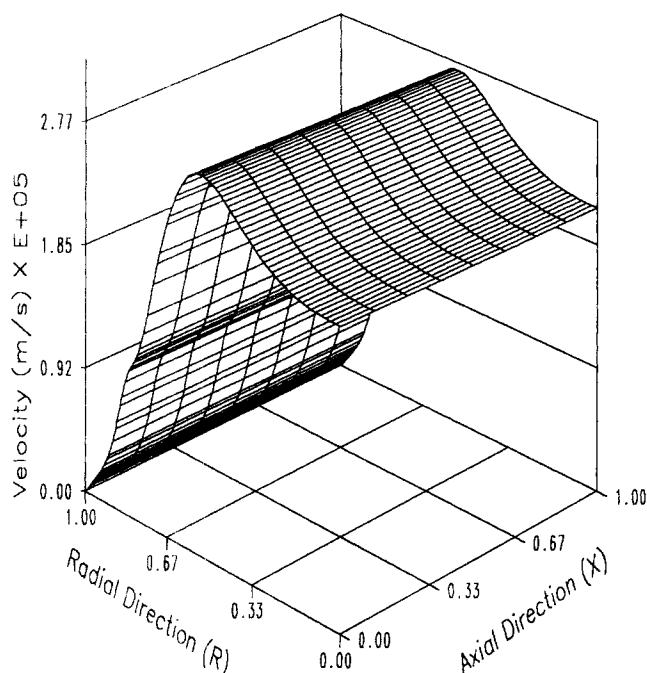
Figure 15. Simulated velocity profile for 0.1 M Na$_2$SO$_4$ at 400 mA.

Radial coordinate: $R = r/a$; axial coordinate: $X = x/L$.

tortuosities are computed from the ratio of free-solution coion diffusivities to the experimentally-determined coion diffusivities.

The mathematical model is tested by comparing predicted and experimental flux rates for simple coion diffusion and electroosmotic solvent transport using aqueous alkali-metal sulfate solutions and a Nafion 117 membrane. Accurate predictions are obtained for electroosmotic water transport during the passage of low currents, and qualitative agreement with experimental data is observed for high-current conditions. The model predicts accurately coion transport rates for diffusion experiments with a pore radius in the range of 25 to 50 Å. When hydration effects and a variable dielectric constant are removed from the model, electrostatic interactions in the ion-exchange membrane pore are rendered inaccurate; coion exclusion is underestimated, and computed coion fluxes are significantly greater than those observed experimentally. The results of this work provide useful insights into the interrelationship between the molecular-level structure of the membrane and the equilibrium absorption and transport of solute and solvent.

Acknowledgment

Notation

a = pore radius, Å
A = hydration constant, J/kmol
B = Bruggeman constant
c = concentration, kmol/m^3 of solution
d = diameter of a Nafion disk, m
$\mathcal{D}$ = infinite dilution diffusion coefficient, m^2/s
D = diffusion coefficient, m^2/s
F = Faraday's constant, 9.6487×10^7 C/kequiv
i = current density, Amp/m^2
IEC = ion exchange capacity, mequiv/g
k = Boltzmann constant, 1.380×10^{-23} J/K
K = partition coefficient of the species, $c_{\text{membrane}}/c_{\text{bulk}}$
m = number of dissolved species
M = molarity of solution, kmol/m^3
n = solvent (water) refractive index, 1.33
$\mathcal{N}$ = Avogadro's number, 6.022×10^{-23} mol^{-1}
N = molar flux, kmol/s $\cdot$ m^2 of wet membrane
p = pressure, Pa
r = radial position within pore, m
r_h = hydration radius, Å
r_p = Pauling crystallographic radius, Å
R = universal gas constant, 8.314×10^{23} J/kmol $\cdot$ K
S = superficial membrane area normal to direction of flow, m^2
T = absolute temperature, K
u = mobility, m$^2 \cdot$ kmol/J $\cdot$ s
v = velocity, m/s
V = volume, m^3
x = axial position within pore, m
z = charge number

Greek letters

Δ = solvation sheath thickness, Å
ϵ = solvent dielectric constant
ε = vacuum permittivity, 8.8542×10^{-12} farad/m
η = water dipole moment, 6.87 C $\cdot$ m
θ = membrane porosity
κ = solution conductivity, mho/m
λ = ionic conductance, mho $\cdot$ m^2/equiv
μ = solvent viscosity, kg/m $\cdot$ s
ρ = solution density, 1,000 kg/m^3
ρ_e = charge density of ions in solution, C/m^3
σ = wall charge density, C/m^2
τ = membrane tortuosity
ϕ = electric potential, V

Subscripts

bulk = bulk properties
dry = conditions of dry membrane
H$_2$O = membrane equilibrated in pure water
j = ionic species
o = water
r = radial component of variable
wet = conditions of wet membrane
x = axial component of variable

Superscripts

o = centerline values

Literature Cited

Andrade, E. N. da C., and C. Dodd, "The Effect of an Electric Field on the Viscosity of Liquids," *Proc. Roy. Soc. London,* **A1877,** 296 (1946).

Babchin, A. J., M. A. Piliavin, and V. G. Levich, "Rheoelectric Effect in a Polar Liquid Interphase Layer," *J. Coll. Int. Sci.,* **57**(1), 1 (1976).

Babchin, A. J., and A. L. Frenkel, "Concentration Gradient Driven Flow of Electrolyte Solution Through a Capillary Membrane: I. Zero Current Case," *J. Coll. Int. Sci.,* **106**(2), 410 (1985).

Booth, F., "The Dielectric Constant of Water and the Saturation Effect," *J. Chem. Phys.,* **19,** 391 (1951).

Born, M., "Volumen und Hydratationswärme der Ionen," *Z. Physik,* **1,** 45 (1920).

Bruggeman, D. A. G., "Berechnung verschiedener physikalischer Konstanten von heterogenen Substanzen: I. Dielektrizitätskonstanten und Leitfähigkeiten der Mischkörper aus isotropen Substanzen," *Annalen der Phys.,* **24,** 636 (1935).

Capeci, S. W., P. N. Pintauro, and D. N. Bennion, "The Molecular-Level Interpretation of Salt Uptake and Anion Transport in Nafion Membranes," *J. Electrochem. Soc.,* **136**(10), 2876 (1989).

Carnahan, B., H. A. Luther, and J. O. Wilkes, *Applied Numerical Methods*, Wiley, New York (1969).

Chandran, R. R., R. S. Yeo, and D. T. Chin, "Sorption and Transport Behavior of Perfluorinated Ionomer Membranes in Concentrated NaOH Solutions," *Electrochim. Acta*, **36**(12), 1585 (1985).

Cotton, F. A., and C. Wilkinson, *Advanced Inorganic Chemistry*, 3rd ed., Interscience Publishers, New York (1972).

Cwirko, E. H., and R. G. Carbonell, "Transport of Electrolytes in Charged Pores: Analysis Using the Method of Spatial Averaging," *J. Coll. Int. Sci.*, **129**(2), 513 (1989).

———, "A Theoretical Analysis of Donnan Dialysis Across Charged Porous Membranes," *J. Memb. Sci.*, **48**, 155 (1990).

Dresner, L., and K. A. Kraus, "Ion Exclusion and Salt Filtering with Porous Ion-Exchange Materials," *J. Phys. Chem.*, **67**, 990 (1963).

Eisenberg, A., and H. L. Yeager, eds., *Perfluorinated Ionomer Membranes, ACS Symp. Ser.*, **180** (1982).

Epstein, N., "On Tortuosity and the Tortuosity Factor in Flow and Diffusion through Porous Media," *Chem. Engr. Sci.*, **44**, 777 (1989).

Escoubes, M., and M. Pineri, "Thermodynamic Studies of the Water-Perfluorosulfonated Polymer Interaction," *Perfluorinated Ionomer Membranes*, A. Eisenberg and H. L. Yeager, eds., *ACS Symp. Ser.*, **180** (1982).

Fair, J. C., and J. F. Osterle, "Reverse Electrodialysis in Charged Capillary Membranes," *J. Chem. Phys.*, **54**(8), 3307 (1971).

Fioshin, M. M., L. A. Shutova, and L. I. Krishtalik, "Ion and Water Transfer across MF-4SK Cation-Exchange Membranes in Concentrated Alkalis," *Soviet Electrochem.*, **22**, 763 (1986); translated from *Élektrokhimiya*, **22**, 814 (1986).

Franks, F. ed., *Water a Comprehensive Treatise*, **3**, Plenum Press (1973).

Gabler, R., *Electrical Interactions in Molecular Biophysics*, Academic Press, New York (1978).

Gierke, T. D., *"Ionic Clustering in Nafion Perfluorosulfonic Acid Membranes and Its Relationship to Hydroxyl Rejection and Chloro-Alkali Current Efficiency*, Meeting of the Electrochemical Society (Oct., 1977).

Gierke, T. D., and W. Y. Hsu, "The Cluster-Network Model of Ion Clustering in Perfluorosulfonated Membranes," *Perfluorinated Ionomer Membranes*, A. Eisenberg and H. L. Yeager, eds., *ACS Symp. Ser.*, **180** (1982).

Gierke, T. D., G. E. Munn, and F. C. Wilson, "Morphology of Perfluorosulfonated Membrane Products," *Perfluorinated Ionomer Membranes*, A. Eisenberg and H. L. Yeager, eds., *ACS Symp. Ser.*, **180** (1982).

Gross, R. J., and J. F. Osterle, "Membrane Transport Characteristics of Ultrafine Capillaries," *J. Chem. Phys.*, **49**(1), 228 (1968).

Gur, Y., I. Ravina, and A. J. Babchin, "On the Electrical Double Layer Theory I.-A Numerical Method for Solving a Generalized Poisson-Boltzmann Equation," *J. Coll. Int. Sci.*, **64**(2), 326 (1978a).

———, "On the Electrical Double Layer Theory II.-The Poisson-Boltzmann Equation Including Hydration Forces," *J. Coll. Int. Sci.*, **64**(2), 333 (1978b).

Helfferich, F., *Ion Exchange*, McGraw-Hill, New York (1962).

Herrera, A., and H. L. Yeager, "Halide and Sulfate Ion Diffusion in Nafion Membranes," *J. Electrochem. Soc.*, **134**, 2446 (1987).

Hodgson, T. D., "Selective Properties of Cellulose Acetate Membranes Towards Ions in Aqueous Solutions," *Desalination*, **8**, 99 (1970).

Kobatake, Y., and H. Fujita, "Flows Through Charged Membranes. I.-Flip-Flop Current vs. Voltage Relation," *J. Chem. Phys.*, **40**(8), 2212 (1964).

Koh, W. H., and J. L. Anderson, "Electroosmosis and Electrolyte Conductance in Charged Microcapillaries," *AIChE J.*, **21**(6), 1176 (1975).

Lakshminarayanaiah, N., *Transport Phenomena in Membranes*, Academic Press, New York (1969a).

———, "Electroosmosis in Ion-Exchange Membranes," *J. Electrochem. Soc.*, **116**, 338 (1969b).

Lapidus, L., and G. F. Pinder, *Numerical Solution of Partial Differential Equations in Science and Engineering*, Wiley, New York (1982).

Latimer, W. M., K. S. Pitzer, and C. M. Slansky, 'The Free Energy of Hydration of Gaseous Ions and the Absolute Potential of the Normal Calomel Electrode," *J. Chem. Phys.*, **7**, 108 (1939).

Lindheimer, A., J. Molenat, and C. Gavach, 'A Study of the Superselectivity of Nafion Perfluorosulfonic Membranes," *J. Electroanal. Chem.*, **216**, 71 (1987).

Morrison, F. A., and J. F. Osterle, "Electrokinetic Energy Conversion in Ultrafine Capillaries," *J. Chem. Phys.*, **43**, 2111 (1965).

Newman, J. S., *Electrochemical Systems*, Prentice-Hall, Englewood Cliffs, NJ (1973).

Noyes, R. M., "Thermodynamics of Ion Hydration as a Measure of Effective Dielectric Properties of Water," *J. Amer. Chem. Sci.*, **84**, 513 (1962).

———, "Assignment of Individual Ionic Contributions to Properties of Aqueous Ions," *J. Amer. Chem. Soc.*, **86**, 971 (1964).

Pintauro, P. N., and M. W. Verbrugge, 'The Electric Potential Profile in Ion-Exchange Membrane Pores," *J. Memb. Sci.*, **44**, 197 (1989).

Powell, R. E., and W. M. Latimer, "The Entropy of Aqueous Solutions," *J. Chem. Phys.*, **19**, 1139 (1951).

Ravina, I., and Y. Gur, "Rheological Model of Pore Water," *J. Rheol.*, **29**(2), 131 (1985).

Rieke, P. C., and N. E. Vanderborgh, "Thin Film Electrode Arrays for Mapping the Current-Voltage Distributions in Proton-Exchange-Membrane Fuel Cells," *J. Electrochem. Soc.*, **134**, 1099 (1987).

Robinson, R. A., and R. H. Stokes, *Electrolyte Solutions*, London Butterworths, 2nd ed. (1959).

Scherer, J. R., and G. F. Bailey, "Water in Polymer Membranes. Part II. Raman Scattering from Guided Laser Beams," *J. Memb. Sci.*, **13**, 43 (1983).

Sparnaay, M. J., "Ion-Size Corrections of the Poisson-Boltzmann Equations," *J. Electroanal. Chem.*, **37**, 65 (1972).

Stokes, R. H., "The Van Der Waals Radii of Gaseous Ions of the Noble Gas Structure in Relation to Hydration Energies," *J. Amer. Chem. Soc.*, **86**, 979 (1964).

Verbrugge, M. W., "Methanol Diffusion in Perfluorinated Ion-Exchange Membranes," *J. Electrochem. Soc.*, **136**, 417 (1989).

Verbrugge, M. W., and R. F. Hill, "Experimental and Theoretical Investigation of Perfluorosulfonic Acid Membranes Equilibrated with Aqueous Sulfuric Acid Solutions," *J. Phys. Chem.*, **92**(23), 6778 (1988).

———, "Ion and Solvent Transport in Ion-Exchange Membranes II. A Radiotracer Study of the Sulfuric-Acid, Nafion-117 System," *J. Electrochem. Soc.*, **137**(3), 893 (1990).

Verbrugge, M. W., and P. N. Pintauro, "Transport Models for Ion-Exchange Membranes," *Modern Aspects of Electrochemistry*, **19**, Plenum Press (1989).

Walton, C. W., and R. E. White, "Modeling of Bilayer Cation Exchange Membranes with Application to Chlor-Alkali Cells," Paper No 409C, AIChE Meeting, Houston (Mar., 1987).

Wang, C. R. C., J. W. Strojek, and T. Kuwana, "Spectrophotometric Measurements of Cation Transport in Nafion," *J. Phys. Chem.*, **91**(13), 3606 (1987).

Weast, R. C., and M. J. Astle, eds., *Handbook of Chemistry and Physics*, CRC Press, 60th ed. (1980).

Westermann-Clark, G. B., and J. L. Anderson, "Experimental Verification of the Space-Charge Model for Electrokinetics in Charged Microporous Membranes," *Electrochem. Sci. and Technol. J. Electrochem. Soc.*, **130**(4), 839 (1983).

Yeo, R. S., "Ion Clustering and Proton Transport in Nafion Membranes and Its Applications as Solid Polymer Electrolyte," *J. Electrochem. Soc.*, **130**(3), 533 (1983).

Yeo, R. S., and D. T. Chin, "A Hydrogen-Bromine Cell for Energy Storage Applications," *J. Electrochem. Soc.*, **127**(3), 549 (1980).